



# Echinacoside Inhibits Osteoclast Function by Down-Regulating PI3K/Akt/C-Fos to Alleviate Osteolysis Caused by Periprosthetic Joint Infection

Tao Jiang<sup>1,2†</sup>, Hanwen Gu<sup>2†</sup> and Jian Wei<sup>1\*</sup>

<sup>1</sup>Department of Joint Orthopedics, Affiliated Liutie Central Hospital of Guangxi Medical University, Liuzhou, China, <sup>2</sup>Department of Orthopedic Surgery, Zhongnan Hospital of Wuhan University, Wuhan, China

## OPEN ACCESS

### Edited by:

Bekir Cinar,

Clark Atlanta University, United States

### Reviewed by:

Yun Liu,

Guangxi Medical University, China

Yan Wang,

Shenzhen Institutes of Advanced Technology, (CAS), China

### \*Correspondence:

Jian Wei

wei198206@163.com

<sup>†</sup>These authors have contributed equally to this work

### Specialty section:

This article was submitted to Experimental Pharmacology and Drug Discovery,

a section of the journal Frontiers in Pharmacology

Received: 27 April 2022

Accepted: 06 June 2022

Published: 24 June 2022

### Citation:

Jiang T, Gu H and Wei J (2022) Echinacoside Inhibits Osteoclast Function by Down-Regulating PI3K/Akt/C-Fos to Alleviate Osteolysis Caused by Periprosthetic Joint Infection. *Front. Pharmacol.* 13:930053. doi: 10.3389/fphar.2022.930053

Infected osteolysis as a common secondary osteoporosis is associated with excessive osteoclastogenesis and bone resorption. The inhibition of osteoclastogenesis and bone resorption have been demonstrated an effective approach in the treatment of osteolytic diseases. Echinacoside (ECH) is a natural phenylethanoid glycoside with multiple biological functions, including anti-inflammatory, antioxidant, and osteoblast differentiation promotion. However, the effects of ECH on osteoclast differentiation and bone resorption function remain unknown. *In vitro*, we investigated the effects of ECH on osteoclast differentiation and bone resorption induced by RANKL and its potential mechanisms. *In vivo*, we established a periprosthetic joint infection (PJI) rat model and demonstrated the changes of infected osteolysis and osteoclasts activities in surgical sites. ECH (20 mg/kg) was injected intraperitoneally after debridement for 4 weeks. Radiological evaluation and bone histomorphometric analysis was performed to assess the efficacy of ECH. The results showed that ECH inhibited osteoclast differentiation, F-actin belts formation, bone resorption function and osteoclast-specific gene expression by preventing NFATc1 translocation, down-regulating its expression and affecting the PI3K/Akt/c-Fos pathway *in vitro*. ECH also alleviated *in vivo* PJI-induced osteolysis and maintained bone mass by inhibiting osteoclast activity. Our study indicated that ECH attenuated RANKL-induced osteoclastogenesis and PJI-induced bone loss and was shown as a potentially effective therapeutic agent for osteoclast-related bone diseases.

**Keywords:** infected osteolysis, echinacoside, osteoclast, periprosthetic joint infection, bone loss

## 1 INTRODUCTION

Periprosthetic joint infection (PJI) is one of the most serious and devastating complications after total joint arthroplasty (TJA) surgery, which severely affects the quality of patients' life and brings a heavy medical burden (Cahill et al., 2008; Aggarwal et al., 2014). Anti-infective therapy is the mainstay of clinical practice in the PJI treatment because the most fundamental pathological manifestations of PJI are infection and inflammation (Romano et al., 2011; Hodges et al., 2021). However, the bone mass of patients with PJI has not received much attention, especially after revision surgery. Several studies have shown that some inflammatory diseases such as infected osteomyelitis (Dapunt et al.,

2015), tuberculosis (Liu et al., 2020), and corona virus disease (Awosanya et al., 2022) promote bone resorption by affecting osteoclasts and developing to secondary osteoporosis. Therefore, PJI-induced inflammation may contribute to the development of osteoporosis by altering osteoclast function.

Echinacoside (ECH), a natural phenylethanoid glycoside, is the main active ingredient presenting in *Cistanche salsa*, which has been reported to be extensively studied in neuroprotection (Lu et al., 2016), antitumor (Ye et al., 2019), anti-aging (Wu et al., 2019), and myocardial remodeling (Ni et al., 2021), antioxidant (Chuang et al., 2022), anti-apoptotic (Zhang et al., 2017), and anti-inflammatory (Zhou et al., 2020). Studies have demonstrated that ECH alleviates hypoxia-induced memory impairment (Zheng et al., 2019), inhibits the development of breast cancer (Bian et al., 2021), alleviates inflammatory bowel disease (Li et al., 2018), and improves heart failure by reversing myocardial remodeling (Ni et al., 2021). ECH has also been found to promote bone formation by enhancing osteoblast proliferation and differentiation as well as alleviating the reduction in bone mass caused by diabetes (Gong et al., 2019) or ovariectomy (Liu et al., 2019). To our knowledge, the effects of ECH on osteoclast differentiation and bone resorption of infected osteolysis remain unknown.

Herein, this study aimed to explore the effects of ECH on osteoclasts differentiation and bone resorption function *in vitro* and *in vivo*, and investigate the regulatory mechanisms of ECH treatment by using an established PJI rat model (Wei et al., 2021a; Wei et al., 2021b), to provide an important experimental basis for elucidating the role and mechanism of ECH in infected-induced osteolysis and important practical implications for guiding the treatment of clinical PJI patients.

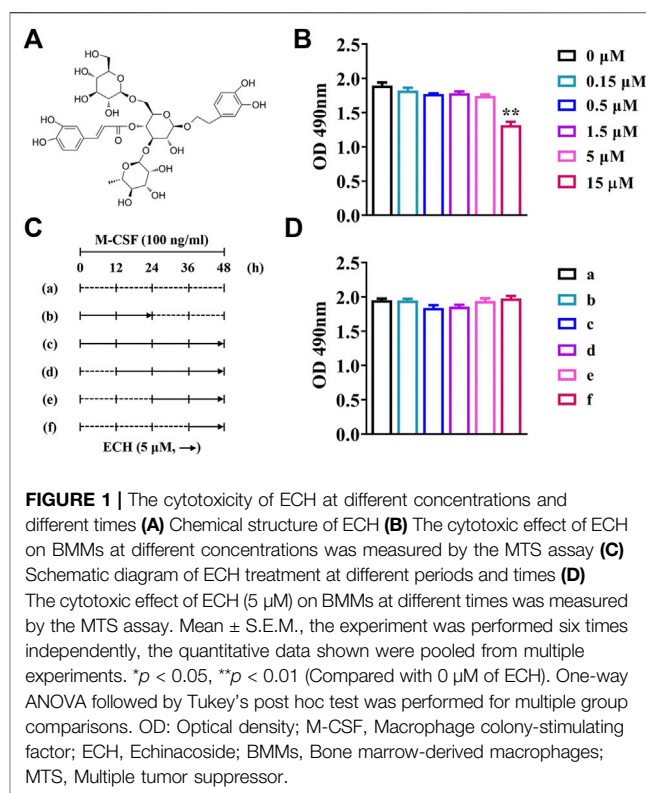
## 2 MATERIAL AND METHODS

### 2.1 Osteoclast Culture

Fresh primary bone marrow cells were extracted from lower limb bone of 4 weeks old rat. Briefly, under aseptic conditions, long bone tissue from the lower extremities of rats was cut and the bone marrow cavity was flushed with PBS (Servicebio, China) until it turned from red to white. The fluid was collected and centrifuged, and then the supernatant was discarded. The cells were lysed with erythrocyte lysate (Servicebio, China) for 10 min and centrifuged again, then the supernatant was discarded. After washing the cells twice with PBS, the cells were resuspended with a complete medium supplemented and then inoculated in culture flasks. 24 h later, the flask liquid was collected, centrifuged and the supernatant discarded to obtain cells, which were cultured for 3 d in a complete medium supplemented with 100 ng/ml M-CSF (MedCemExpress, United States) to obtain bone marrow-derived macrophages (BMMs). Then, we induced BMMs differentiation with 100 ng/mL M-CSF and 50 ng/ml RANKL (R&D systems, United States) for 4 d.

### 2.2 Cytotoxicity Assay

The 3-(4,5-dimethyliazol-2-yl)-5-(3-carboxymethoxyphenyl)-2-(4-sulfophenyl)-2H-tetrazolium (MTS) assay kit (Promega,



United States) was used to assess cell proliferation. BMMs ( $3 \times 10^4$  cells/well) were inoculated in 96-well plates and incubated with culture medium (including M-CSF) overnight. Echinacoside (ECH) was commercially purchased from Merck (Germany) and added into the wells as shown in Figure 1. MTS solution (20 μl/well) was added into each well 48 h later and incubated for 2 h at 37°C. The effects of compounds on cells were measured by absorbance at 490 nm using a spectrophotometer (BioTek, United States).

### 2.3 Tartrate-Resistant Acid Phosphatase (TRAP) Staining

In brief, after removing the medium, the cells were fixed by adding 4% paraformaldehyde and the cells membrane was broken by adding 0.1% Triton. After cleaning with PBS, tartrate-containing buffer and chromogenic substrate were added. After incubation at 37°C for 1 h, washing with PBS, redyeing with hematoxylin for 2 min, and washing with ddH<sub>2</sub>O, cells were stained for TRAP enzymatic activity according to the TRAP staining kit scheme (Sigma, United States). NIS Elements BR light microscope (Nikon, Japan) was used for photography, and ImageJ software was used for quantification analyses.

### 2.4 F-Actin Staining

After removing the medium, the cells ( $6 \times 10^4$  cells/well) were fixed by adding 4% paraformaldehyde for 30 min and the cells membrane was broken by adding 0.1% Triton for 10 min. The

**TABLE 1** | Rat oligonucleotide primers and reaction conditions used in qRT-PCR.

Genes	Forward primers (5'-3')	Reverse primers (5'-3')	Annealing (°C)
Acp5	CAAAGAGATCGCCAGAACCG	GAGACGTTGCCAAGGTGATC	60
CtsK	CAGAGGCCACAACCTCAGAA	GTGTCCATCGATGCAAGCTT	60
c-Fos	AGCTCCCACCAAGTGTCTACC	TCACCGTGGGGATAAAGTTGG	60
NFATc1	CCGTTGCTTCCAGAAAATAACA	TGTGGGATGTGAACTCGGAA	60
Oscar	CGATTGGCACAGCAGGCG	AAGACACATGAAGGAAATAGAG	60
Mmp9	TGAAGGCGACCTCAAGTG	GCGGCAAGTCTTCGGTGTAG	60
GAPDH	GCCTCCAAGGAGTAAGAAAC	GTCTGGGATGGAATTGTGAG	60

qRT-PCR, quantitative real-time polymerase chain reaction; Acp5, Acid phosphatase 5; CtsK, Cathepsin K; c-Fos, Protooncogene c-Fos; NFATc1, Nuclear factor of active T cells 1; GAPDH, glyceraldehyde phosphate dehydrogenase.

cells were added F-actin fluorescent dye (Beyotime, China) followed by cleaning with PBS. After incubation at room temperature without light for 30 min and then washing with PBS, the cells were redyed with DAPI for 10 min without light. The cells were imaged using an inverted fluorescence microscope (Nikon, Japan), and ImageJ software was used for quantification analyses.

## 2.5 Bone Resorption Assay *in Vitro*

As for bone resorption, BMMs ( $3 \times 10^3$  cells/well) were cultured on sterile bovine bone plates, using the same culture methods and reagents as before. After 6 days of induction, the cells were rinsed three times with 10% sodium hypochlorite and water. Finally, the scanning electron microscope using Gatan digital camera system (Zeiss, Germany) was used to take pictures, and ImageJ software was used for quantification analyses.

## 2.6 RNA Extraction and Quantitative Real-Time Polymerase Chain Reaction (qRT-PCR)

BMMs were pretreated with gradient concentrations of ECH for 5 days followed by 50 ng/ml RANKL with or without ECH for 12 h. Total RNA from BMMs was extracted utilizing TRIzol reagent (Invitrogen, Carlsbad CA, United States) in accordance with the manufacturer's protocol. The isolated RNA was collected and quantify by Nanodrop 3000 (United States). cDNA was generated from RNA samples using M-MLV reverse transcriptase and oligo dT primers (Promega). RT-qPCR was performed using diluted cDNA. Total RNA from periprosthetic bone tissues was extracted using Trizol reagent. In brief, 20 mg of bone tissues was placed into a 1.5 ml EP tube, with 3 zirconia beads and 1 ml of Trizol. The EP tubes were placed in a homogenizer (China; 60HZ, 4 min, 4°C). After sufficient homogenization, the EP tube was added with 200  $\mu$ l of chloroform and shaken vigorously for 30 s, and then placed on ice for about 10–15 min. After centrifugation (12000 rpm, 4°C, 15 min), the supernatants were carefully aspirated and transferred to a new EP tube, with an equal volume of isopropanol, mixing the mixture upside down and then leave at room temperature for 10 min after centrifugation (12000 rpm  $\times$  10 min, 4°C), the supernatant was carefully discarded. After centrifugation (12000 rpm  $\times$  10 min,

4°C), the supernatant was carefully discarded and the RNA precipitate was retained. The RNA was then washed twice with pre-cooled 75% ethanol and finally mixed with appropriate amount of ultrapure water. The isolated RNA, generated cDNA and RT-qPCR procedure was performed following the above protocol. The PCR primers for amplification of rat, including Acid phosphatase 5 (Acp5), Cathepsin K (CtsK), Protooncogene c-Fos (c-Fos), Nuclear factor of active T cells 1 (NFATc1), and glyceraldehyde phosphate dehydrogenase (GAPDH) are presented in **Table 1**. All primers were synthesized by Sangon Biotech (China). The relative amounts of the mRNA levels of the target genes were normalized to GAPDH and calculated by using the  $2^{-\Delta\Delta CT}$  method.

## 2.7 Western Blotting Analysis

Osteoclasts were induced to differentiate 2 d after addition of RANKL. Then cells were changed with fresh medium containing serum and cytokine, and treated with ECH in the meantime. After holding for 2 d, cells were collected with RIPA lysate (Servicebio, China) containing 1% PMSF (Servicebio, China), and then proteins were extracted. The corresponding protein expression in osteoclasts was detected by the western blotting technique. Briefly, after protein quantification, proteins were denatured, separated on SDS-PAGE gels, and transferred onto PVDF membranes (EMD Millipore, Burlington, MA, United States). The membranes were immunoblotted with primary rabbit antibody for PI3K, p-Akt, Akt, c-Fos, NFATc1, and CtsK (diluted 1:1000, respectively; Abclonal, China), primary mouse antibody for GAPDH (diluted 1:5,000; Abclonal, China) overnight at 4°C. The next day, membranes were washed and then incubated with horseradish peroxidase-conjugated secondary antibodies (goat anti-mouse IgG and goat anti-rabbit IgG; diluted 1:5,000, respectively; Abclonal, China) at room temperature for 1 h. Antibodies were detected with enhanced chemiluminescence substrate (PerkinElmer, United States), and ImageJ software was used for quantification analyses.

## 2.8 Immunofluorescence (IF) Analysis

BMMs were fixed with 4% paraformaldehyde under 4°C for 15 min and then added with a blocking solution (10% goat serum-PBS) for 2 h at room temperature. Rabbit anti-c-Fos antibody (diluted 1:100; Abclonal, China) was added and incubated overnight at 4°C in a humid chamber. After

**TABLE 2 |** Allocation of animals per group and investigations are as follows: the surgery, X-ray, and Micro-CT detection are performed in all animals per group; the assigned animals per group of numbers 1 to 5 are used for femur H&E, TRAP, and immunofluorescence staining, while numbers 6 to 10 are used for qRT-PCR.

Analyses	Number of animals
Total animals ( $n = 10$ per group)	1 2 3 4 5 6 7 8 9 10
Arthroplasty surgery	x x x x x x x x x x
X-ray	x x x x x x x x x x
Micro-CT	x x x x x x x x x x
Femur H&E staining	x x x x x
Femur TRAP staining	x x x x x
Femur Immunofluorescence staining	x x x x x
qRT-PCR (periprosthetic bone tissues)	x x x x x

Micro-CT: Micro-Computed Tomography; TRAP: Tartrate-Resistant Acid Phosphatase; H&E: hematoxylin and eosin; qRT-PCR: quantitative real-time polymerase chain reaction.

washing with deionized water 5 times, FITC goat anti-rabbit IgG (H + L) (diluted 1:5,000; Abclonal, China) secondary antibody was incubated in the dark at room temperature for 60 min. The cells were added DAPI, and incubated in the dark for 10 min at room temperature following washing 3 times with PBS, then rinsing with deionized water for 15 min. Images were collected using an inverted fluorescence microscope (Nikon, Japan). The Image-Pro Plus 6.0 (Media Cybernetics, Silver Spring, MD, United States) was used for quantification.

## 2.9 Periprosthetic Joint Infection-Induced Bone Loss Rat Model

The protocol of all animal experiments was approved by the Committee on the Ethics of Animal Experiments of the School of Medicine, Wuhan University. All animal experimental procedures were performed following the Guidelines for the Care and Use of Laboratory Animals of the Chinese Animal Welfare Committee. Forty Wistar rats (male,  $255 \pm 6$  g, 10 weeks old) were supplied by the Animal Experiment Center of Zhongnan Hospital (Wuhan, China). All rats were randomly divided into four groups: Control group (femur prosthesis implantation (FPI) surgery without infection,  $n = 10$ ), PJI group (FPI surgery with infection,  $n = 10$ ), PJI + debridement (DEB) group ( $n = 10$ ), and PJI + DEB + ECH (20 mg/kg) group ( $n = 10$ ). The surgical procedure was performed based on previously described rat PJI models (Wei et al., 2021a; Wei et al., 2021b). Briefly, after general anesthetization by inhalation delivered via nose cone with 2.5% isoflurane, the right legs of all rats were shaved and disinfected. The knee was surgically exposed, and a 1.4-mm hole was drilled into the femoral canal just anterior to the Blumensaat line. The prosthesis (diameter 1.5 mm, length 8 mm) was manually placed through retrograde insertion with a screwdriver, with 1 mm screw cap protruding into the joint. After closing the capsule,  $40 \mu\text{l}$  of  $1.5 \times 10^7$  CFU/ml *S. aureus* (ATCC 25923) was injected into the articular cavity of knee assigned to the PJI rat model. On days 7 after surgery and bacterial inoculation, debridement and retention of the prosthesis procedures were carried out for those rats of PJI + DEB and PJI + DEB + ECH groups. The rats in the PJI + DEB +

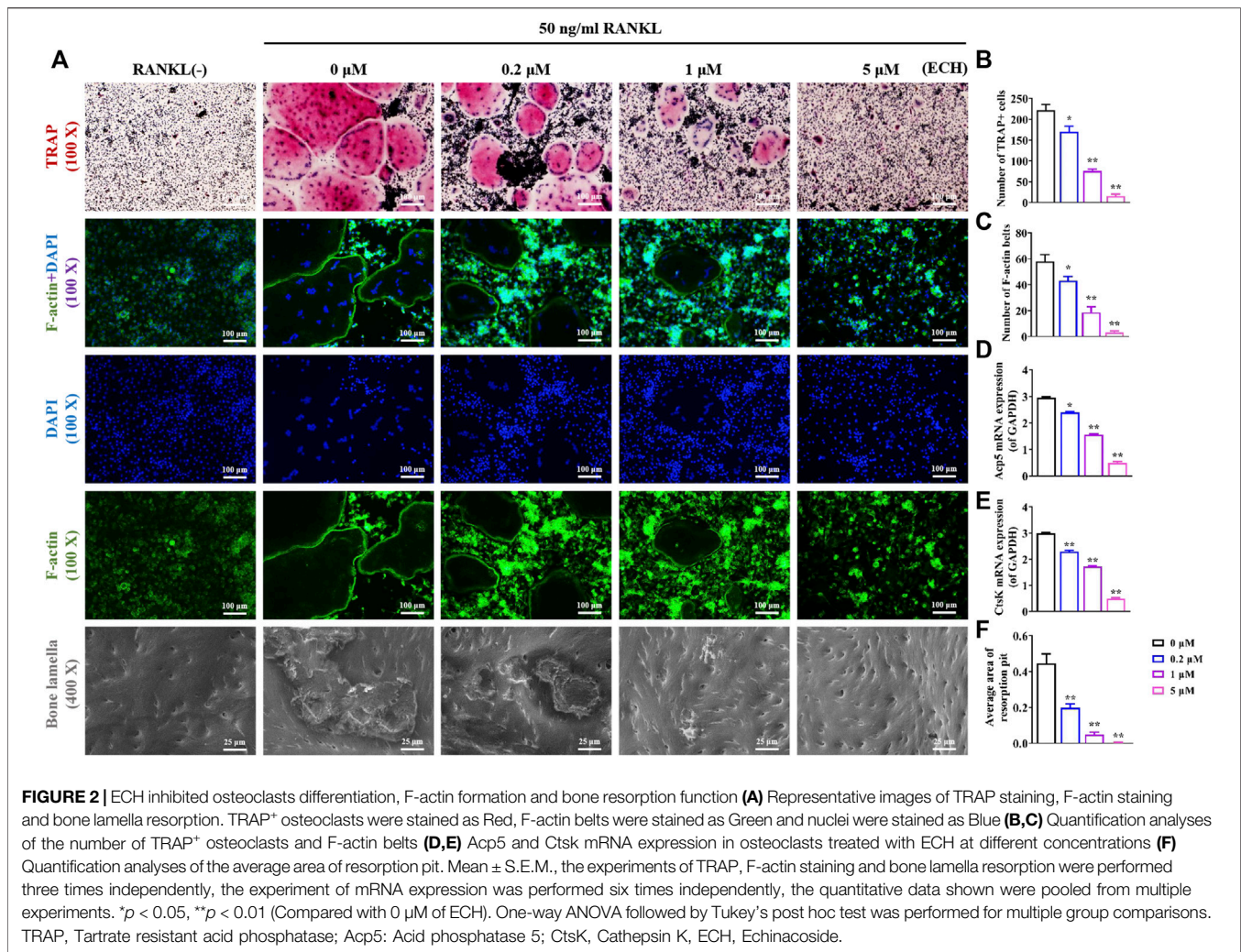
ECH group were intraperitoneally injected of ECH at 20 mg/kg every day for 4 weeks after debridement. The other groups of rats were intraperitoneally injected with PBS as vehicle control. In addition, we have previously performed comparative studies with the PJI rat model and the ovariectomy (OVX) + FPI surgery rat model. Briefly, the animals were divided into three groups: 1) Control group (FPI surgery,  $n = 8$ ), 2) PJI group (FPI surgery with infection,  $n = 8$ ), 3) OVX + FPI group,  $n = 8$ . Micro-CT was carried out at post-surgical 6 weeks to analyze changes in distal femur bone mass around the prosthesis. The results are shown in **Supplementary Figure S1**. Both the PJI group and OVX + FPI group showed a significant reduction in bone mass compared with the control group ( $p < 0.01$ ). However, no statistical differences were observed between the PJI group and OVX + FPI group ( $p > 0.05$ , **Supplementary Figure S1**). Thus, our previous studies suggested that the PJI-induced osteolysis rat model established in this study was reliable. **Table 2** reports the allocation of animals per group and the relative analysis.

## 2.10 X-Ray and Micro-Computed Tomography (Micro-CT)

X-ray images were taken using the Bruker Xtreme BI (Germany; filter: 0.4 mm, 45 kVp, exposure time: 1.2 s, bin:  $1 \times 1$  pixels, F Stop: 2) to determine the position of the prosthesis and osteolysis around the prosthesis. Femur bone was scanned and analyzed by Skyscan1276 micro-CT system (Bruker, Germany) using the following settings: voltage 85 kV; filter 1 mm; current 200  $\mu\text{A}$ ; exposure time 384 ms; image pixel size:  $17.420 \mu\text{m}$ , including bone volume per trabecular volume (BV/TV), trabecular number (Tb. N), trabecular thickness (Tb. Th) and trabecular separation (Tb. Sp). All the above parameters refer to the guidelines of micro-CT for evaluating bone microstructure (Bouxsein et al., 2010).

## 2.11 Bone Histomorphometry Analysis

All samples were fixed in 4% paraformaldehyde for 48 h, then decalcified with EDTA for 28 d, dehydrated, embedded with paraffin, and finally sectioned into  $4 \mu\text{m}$  slices. After the slices were dewaxed and washed in PBS, hematoxylin and eosin (H&E), TRAP and IF staining were performed. H&E staining method for tissue was as follows. Paraffin sections were first dewaxed with xylene and then dehydrated through graded ethanol of decreasing concentration (100%, 90%, 80%, 70%; 5 min/concentration, respectively), hematoxylin staining was performed for 5 min after washing with PBS for 5 min (triplicate), then washing with PBS for 5 min (twice). Eosin staining was performed for 3 min and then washed with PBS for 30 s (twice), and then dehydrated through graded ethanol of increasing concentration (70%, 80%, 90%, 100%; 30 s, respectively). Finally, the slices were rehydrated and sealed with a neutral resin. TRAP staining method for tissue was as follows. Paraffin sections were first dewaxed with xylene and then dehydrated through graded ethanol of decreasing concentration (100%, 90%, 80%, 70%; 5 min/concentration, respectively), washing with PBS for 5 min (triplicate), then



soaked in preheated PBS at 37°C for 10 min, incubated the staining with the prepared TRAP working solution (Sigma, United States) for 2 h at 37°C, followed by washing with PBS 3 times. Hematoxylin staining was performed for 3 min and then washed with PBS. Differentiation and blue return with differentiation and blue return solution was carried out. Finally, the slices were rehydrated and sealed with a neutral resin. For bone tissue IF staining, paraffin sections were first dewaxed to water, then antigen repair was performed in a microwave oven with EDTA antigen repair buffer (medium heating for 3 min, low heating for 10 min). After drawing circles around the tissue with a histochemical pen, 3% BSA (Roche, United States) was added dropwise to the section and blocked for 30 min. The subsequent treatment was referred to the protocols used for cells in section 2.8.

## 2.12 ELISA Assay

Serum samples were obtained by centrifugation (3000 rpm, 4°C, 15 min) at 4 weeks after debridement and ECH treatment. Serum creatinine (Cr), urea nitrogen (UN), alanine

aminotransferase (ALT) and aspartate aminotransferase (AST) of rats in each group were measured by ELISA kit (Huamei Biotech Co., Ltd., China).

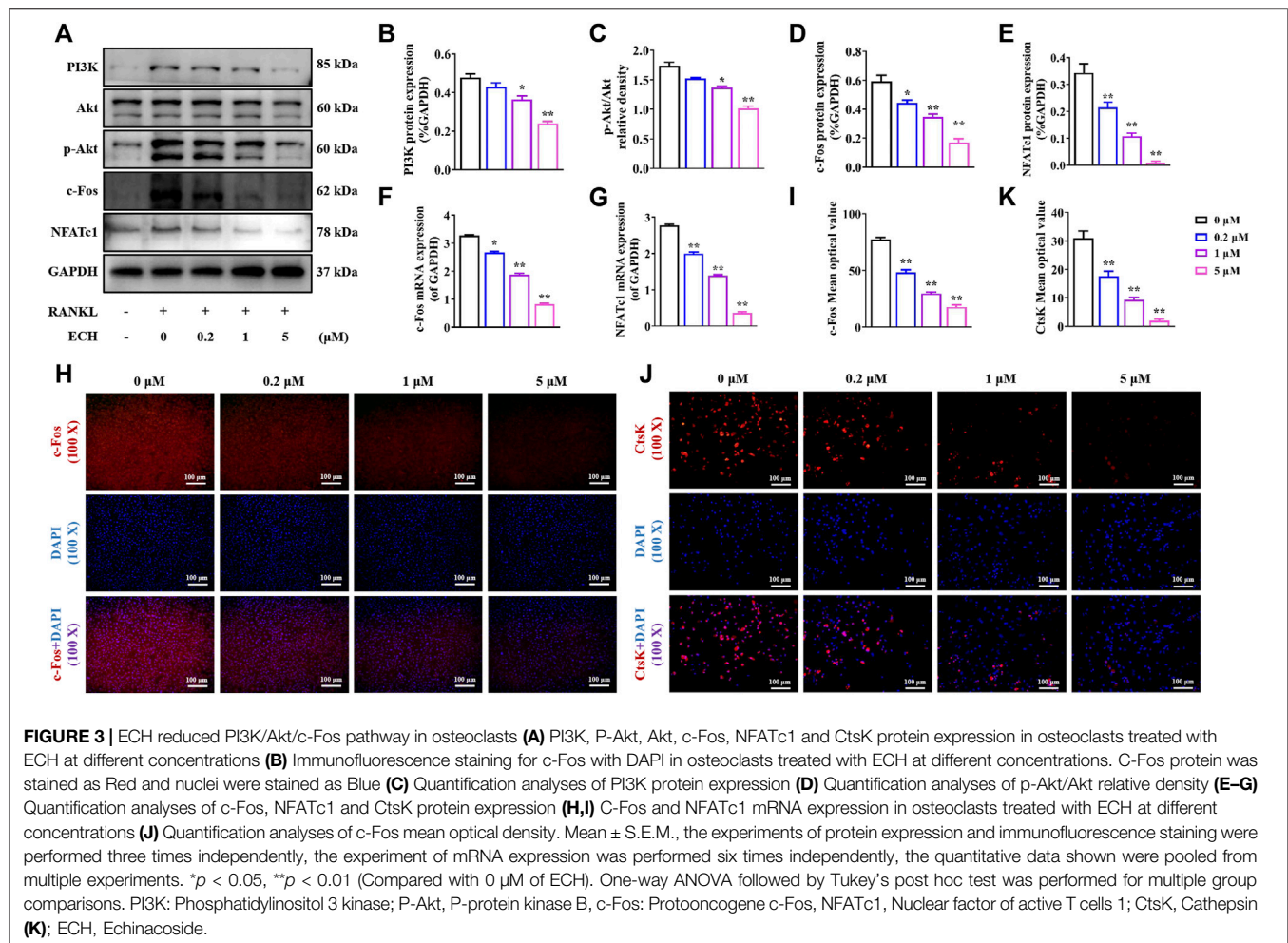
## 2.13 Statistical Analysis

Data were analyzed using GraphPad Prism software (version 8.0, La Jolla, CA, United States). All data were expressed as mean ± standard error of the mean (S.E.M). One-way ANOVA test was used for multi-group comparison, followed by Dunnett *t*-test to determine whether the difference between the two groups was significant. A value of *p* < 0.05 was considered statistically significant.

## 3 RESULTS

### 3.1 Echinacoside Inhibited RANKL-Induced Osteoclast Formation Without Cytotoxicity

The results of the MTS assay showed that no significant inhibition of the proliferation of BMMs was observed when the ECH concentration was no more than 5 μM (*p* < 0.01, Figure 1B). No significant effects of inhibiting the



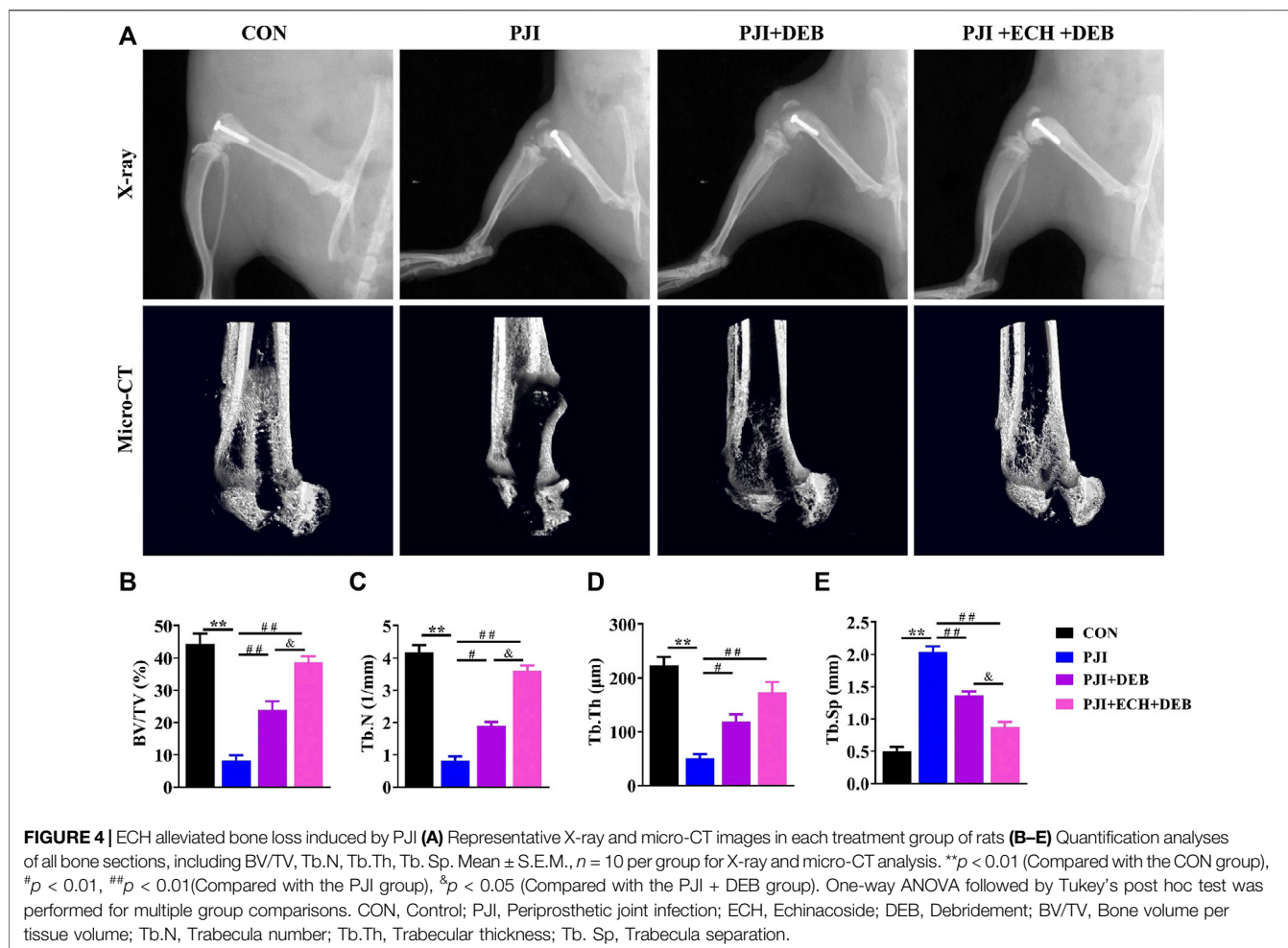
proliferation of BMMs was observed while ECH was given at a concentration of 5  $\mu\text{M}$  both the administration period (early/late) and the duration of administration (12/24/36/48 h) (Figure 1C,D).

As shown in Figure 2A, the addition of RANKL significantly promoted osteoclast differentiation and formation. Besides, an inhibitory effect of different concentrations of ECH on osteoclast differentiation and bone resorption function was detected. TRAP staining results showed that the control group presented mature TRAP<sup>+</sup> osteoclasts. In contrast, osteoclast development was significantly inhibited in the ECH group, along with a concentration-dependent phenomenon (Figure 2A). The visualization indicated that ECH significantly reduced the number of TRAP<sup>+</sup> osteoclasts ( $p < 0.05$ ,  $p < 0.01$ , Figure 2B) and inhibited the expression of the osteoclast marker genes Acp5 and CtsK ( $p < 0.05$ ,  $p < 0.01$ , Figures 2D,E). The F-actin belt is an important symbol of mature osteoclasts, and an intact F-actin belt is necessary for bone resorption function (Sun et al., 2019). To further verify the inhibiting osteoclastogenesis of ECH, we performed the F-actin belt staining assay. The number and mean size of F-actin belts after ECH treatment were significantly lower than those of the control group ( $p < 0.05$ ,  $p < 0.01$ , Figure 2C). The bone plate resorption images were

shown in Figure 2A, the control group presented large resorption pits, while the resorption pits reduced in varying degrees after ECH treatment and showed a concentration-dependent reduction ( $p < 0.01$ , Figure 2F). These data suggested that ECH significantly inhibited RANKL-induced osteoclastogenesis and F-actin belt formation as well as bone resorption function of osteoclasts in the absence of cytotoxicity.

### 3.2 Echinacoside Inhibited Osteoclasts Differentiation and Function by Preventing PI3K/Akt/C-Fos Pathway *in vitro*

PI3K/Akt signaling is an important pathway for RANKL-induced osteoclastogenesis. The RANKL/RANK complex leads to osteoclast PI3K activation and Akt phosphorylation, further upregulating osteoclast-associated important transcription factor protooncogene c-Fos, which mediates osteoclast differentiation and maturation (Baek et al., 2016). It has been found that *Rehmannia Radix Praeparata* which contained ECH could enhance osteoblastic bone formation via PI3K/Akt pathway in diabetic rats (Gong et al., 2019). It has also been confirmed that ECH can induce nitric oxide production via PI3K/Akt pathway in endothelial cells (Gu et al., 2020). ECH can also inhibit the

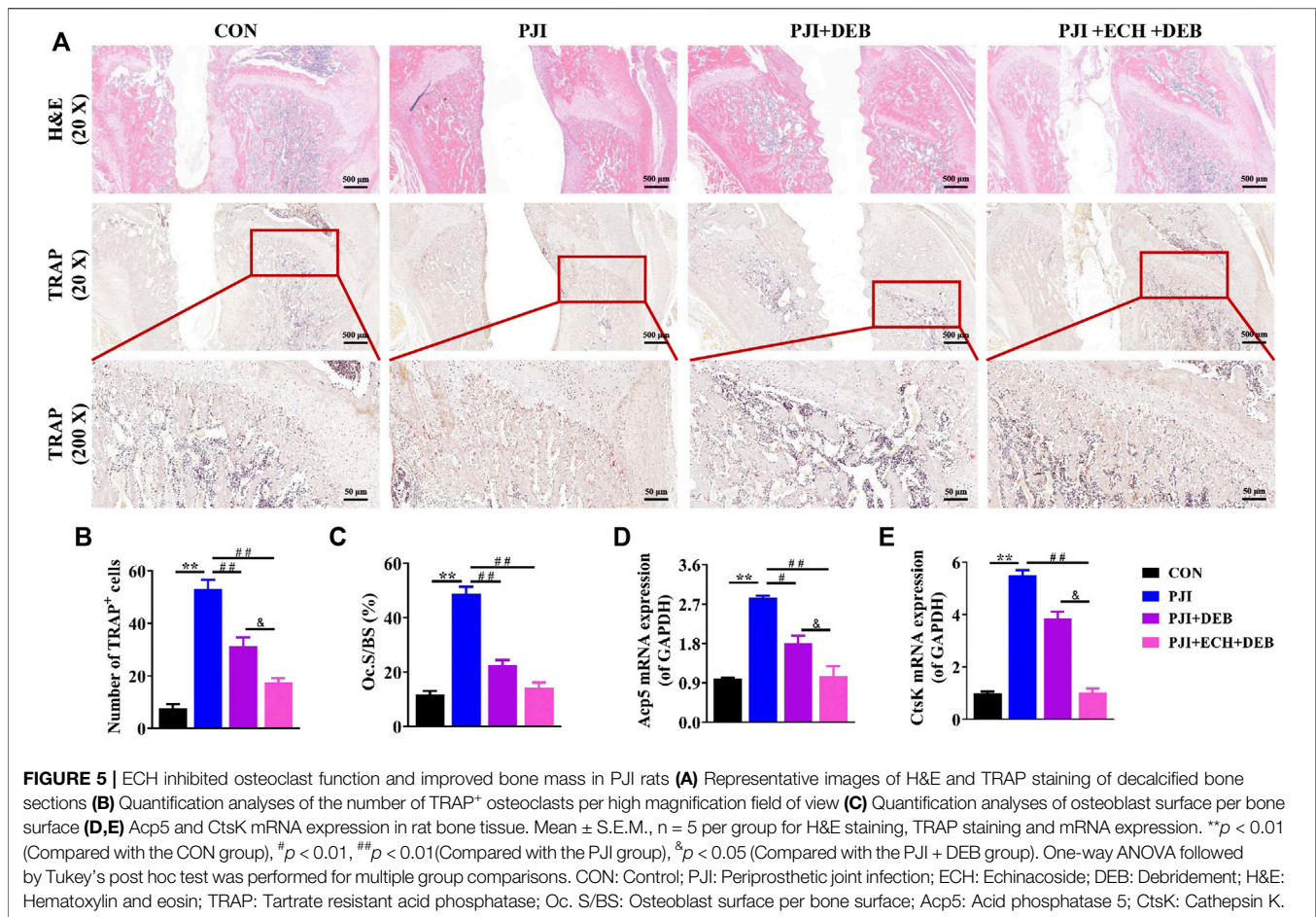


proliferation and migration of ovarian cancer cells via PI3K/Akt/mTOR pathway (Liu et al., 2022). These above studies suggested that PI3K/Akt/c-Fos pathway may be an important downstream pathway of ECH. To further investigate the specific mechanism of inhibiting osteoclast differentiation and function by ECH, we examined the effect of ECH on the PI3K/Akt/c-Fos pathway. As shown in **Figure 3A**, RANKL significantly activated the PI3K/Akt/c-Fos/NFATc1 signaling pathway in osteoblasts. Quantitative results showed that ECH concentration-dependently inhibited PI3K expression and Akt phosphorylation ( $p < 0.05$ ,  $p < 0.01$ , **Figures 3A–C**) and the expression of the c-Fos gene ( $p < 0.05$ ,  $p < 0.01$ , **Figure 3F**) and protein ( $p < 0.05$ ,  $p < 0.01$ , **Figures 3A,D, 3H,I**), further down-regulated the downstream NFATc1 ( $p < 0.01$ , **Figures 3A,E,G**) as well as CtsK expression ( $p < 0.01$ , **Figures 3J,K**). These data suggested that ECH exerted an inhibitory effect on osteoclasts through the PI3K/Akt/c-Fos signaling pathway.

### 3.3 Echinacoside Alleviated Periprosthetic Joint Infection-Induced Bone Loss

After determining the inhibition of osteoclast production and function by ECH, we investigated the inhibitory effect of ECH

on bone erosion of PJI rats and evaluated the potential of ECH as a therapeutic agent for inflammatory osteolysis. We administrated ECH (20 mg/kg) intraperitoneally once daily for 4 weeks after debridement in PJI rats. No adverse effects or deaths were recorded after both PJI modeling and ECH treatment. No obvious structural changes were observed in the kidney and liver of each treatment group (**Supplementary Figure S2A,B**). No significant differences were detected in the serum Cr, UN, ALT and AST among each treatment group ( $p > 0.05$ , **Supplementary Figure S2C–F**). X-rays showed that the PJI group exhibited significant periprosthetic osteolysis compared to the control group (without infection). Osteolysis was significantly alleviated in the DEB combined with ECH treatment group, which was superior to that of the DEB group (**Figure 4A**). Micro-CT images and analysis revealed that a significant increase of bone volume (BV/TV, Tb. N, Tb. Th, and Tb. Sp) were detected in the ECH treatment group compared with the PJI and DEB group, but lower than the control group ( $p < 0.05$ ,  $p < 0.01$ , **Figures 4A–E**). This suggested that ECH treatment significantly improved bone mass of PJI-induced rat model.



### 3.4 Echinacoside Attenuated Osteoclasts Function by Down-Regulating c-Fos/NFATc1 in Periprosthetic Joint Infection Rats

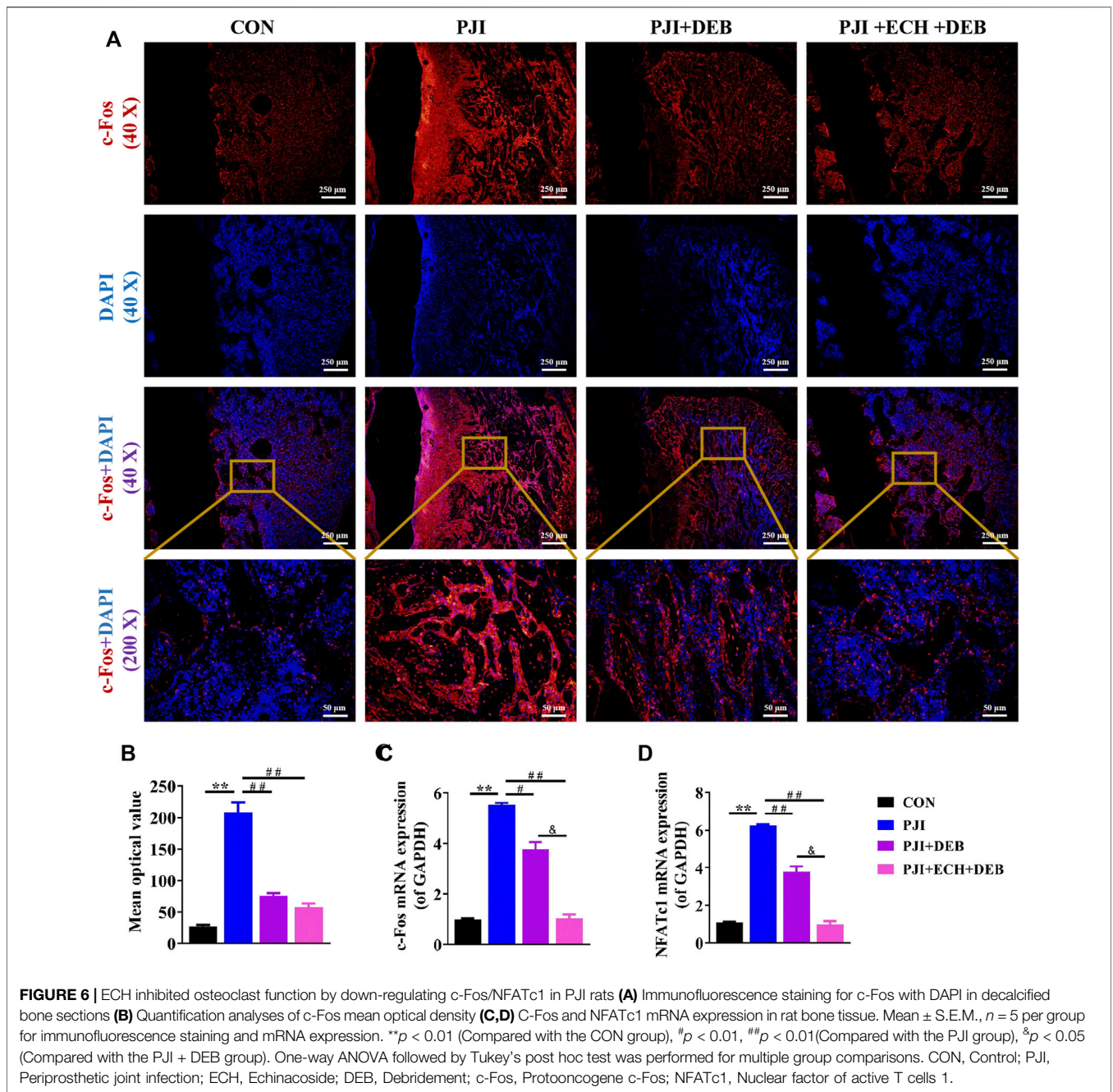
Based on the X-ray and Micro-CT results, we performed a histological study. H&E staining suggested that a significant decrease in bone destruction around the prosthesis were observed in the ECH and DEB treatment group compared with the PJI and DEB group (Figure 5A). TRAP staining and quantitative analysis showed that larger number of TRAP<sup>+</sup> osteoclasts were detected in the PJI group than the control group, while these changes were significantly improved by ECH and DEB treatment ( $p < 0.01$ , Figures 5A,B). The osteoclast surface/bone surface (Oc.S/BS) was significantly reduced ( $p < 0.01$ , Figure 5C), and Acp5 and CtsK gene expression was significantly downregulated ( $p < 0.01$ , Figures 5D,E). These anti-osteoclast effects in ECH and DEB group were better than those of DEB group, but lower than the control group.

Moreover, we examined the effects of ECH on c-Fos/NFATc1 expression *in vivo*. The results showed that both the gene and protein expression of c-Fos and NFATc1 were significantly upregulated in the PJI group compared with the control group, while these changes were significantly inhibited after

DEB and ECH and DEB treatment. The inhibitory effects of ECH and DEB group were stronger than that in the DEB group alone ( $p < 0.01$ , Figures 6A–D). The above data indicated that ECH significantly reduced osteoclast function and alleviated the PJI-induced bone loss by downregulating c-Fos/NFATc1.

## 4 DISCUSSION

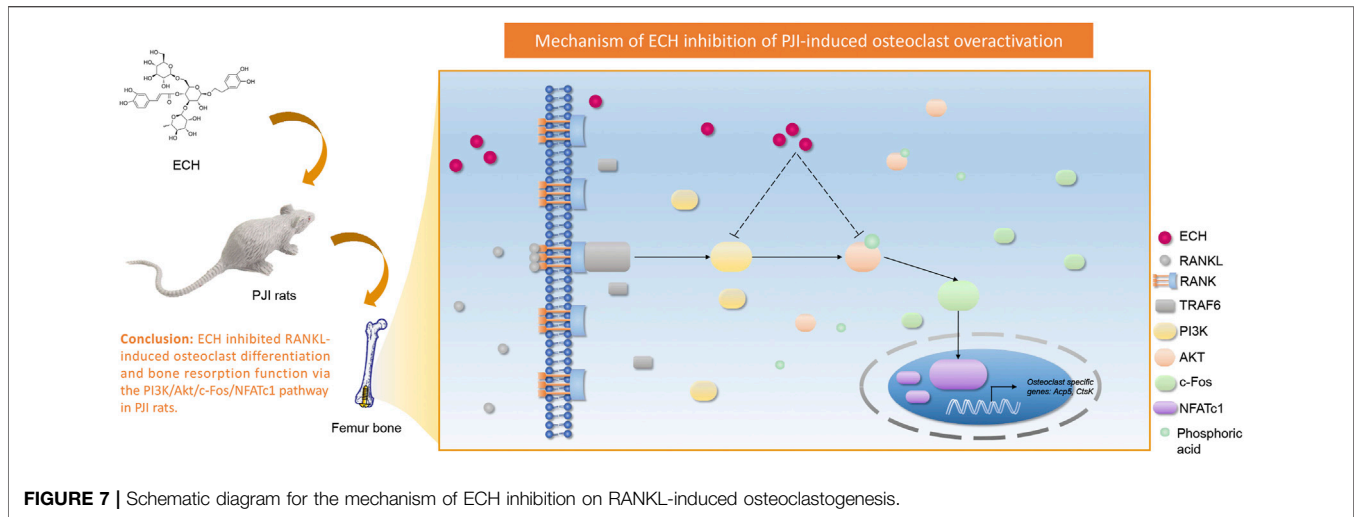
In recent years, an increasing number of studies have found that infections or aseptic inflammatory conditions (e.g., infected osteomyelitis, septic arthritis, AIDS, rheumatoid arthritis, and inflammatory bowel disease) can contribute to the development of secondary osteoporosis (Sakurai et al., 2003; Mundy, 2007; Dapunt et al., 2015; Gallego-Escuredo et al., 2017; Rychter et al., 2021). Redlich introduced the concept of inflammatory bone loss, namely inflammation causes bone loss by disrupting bone metabolism, activating bone degradation, and inhibiting bone remodeling (Redlich and Smolen, 2012). The occurring of inflammatory diseases might bring systemic effects on the bone mass as well as increase the risk of osteoporosis and fracture. Thus, the potential pathogenesis and signal pathways of inflammatory bone loss, as well as exploring effective therapeutic agents attract the attention of the scholars



increasingly. In this study, we investigated the pathogenesis and potential therapeutic agents of inflammatory bone loss caused by infection using the PJI rat model as an entry point. We observed severe osteolysis with abnormal hyperfunction of osteoclasts in the PJI rat model. Administration of ECH to PJI rats resulted in a significant reduction in bone loss and significant inhibition of osteoclast function. This study expanded the concept of inflammatory bone loss and provided a theoretical and experimental basis for strategies to prevent and treat inflammatory osteolysis.

Most current studies point to the emerging anti-inflammatory and neuroprotective effects of ECH(Zhou et al., 2020; Zeng et al.,

2021). It had been reported that ECH could promote osteoblast mineralization through upregulation of OPG/RANKL (Li et al., 2012) and osteoblast proliferation and differentiation through the Wnt/ $\beta$ -catenin signaling pathway (Tang et al., 2020). Therefore, based on the above studies, we speculated and confirmed that ECH have a potential anti-osteoclast function in this study. TRAP staining is a standard method used to detect osteoclast differentiation (Hayman, 2008), and the F-actin belt is the most distinctive feature of mature osteoclasts (Marchisio et al., 1984), as well as the bone plate resorption assay is used to measure the bone resorption capacity of osteoclasts. In the present experiment, the concentration-dependently inhibition



of ECH in the RANKL-induced osteoclast differentiation and activity was observed. F-actin staining showed that ECH exhibited concentration-dependent inhibition of osteoclast F-actin belts formation. The *in vitro* bone resorption results indicated that ECH significantly inhibited the formation of pits in the bone plate, with a concentration-dependent attenuation effect. According to the above data of anti-osteoclast function by ECH, we further performed ECH intervention treatment on the PJI rat model. After debridement and 4-week intraperitoneal injection of ECH, the bone mass of PJI rats was significantly improved, accompanied by down-regulation of c-Fos expression and significant inhibition of osteoclast function. Thus, these results confirmed the emerging role of ECH in inhibiting osteoclast function and alleviating infected osteolysis.

Several studies have identified an important role for the PI3K/Akt/c-Fos pathway in the regulation of osteoclast function (Suh et al., 2013; Li et al., 2020). During the early stages of osteoclastogenesis, the binding of RANKL secreted by osteoblasts to the osteoclast precursor cell membrane receptor RANK activates several molecular transduction pathways, including MAPK, NF- $\kappa$ B, PI3K/Akt, and others (Jia et al., 2019). Among these signaling pathways, the PI3K/Akt signaling cascade regulates c-Fos expression during osteoclastogenesis, which in turn regulates osteoclast function (Yeon et al., 2019). Increasing phosphorylation of Akt promoted c-Fos activation significantly (Han and Kim, 2019), while c-Fos knockout mice exhibited significant downregulation of osteoclast marker genes (Acp5, CtsK, etc.) (Fleischmann et al., 2000). Various drugs such as Idelalisib, Asperolide A, Garcinol, and Ebselen have been proven to inhibit osteoclast function via the PI3K/Akt/c-Fos pathway and exert an anti-osteolysis effects (Suh et al., 2013; Baek et al., 2016; Yeon et al., 2019; Jiang et al., 2020).

In this study, we found that ECH could inhibit the PI3K/Akt/c-Fos pathway in osteoclasts by downregulating PI3K expression, decreasing Akt phosphorylation levels, and decreasing c-Fos expression. NFATc1 is a specific transcription factor that

regulates osteoclast-specific genes (Acp5, CtsK, etc.) and RANKL/RANK complex-mediated osteoclast differentiation and functional activation (Ahern et al., 2018). The present data indicated that ECH treatment significantly reduced RANKL-induced NFATc1 activation and the expression of downstream target genes Acp5 and CtsK. Therefore, these results confirmed that the inhibitory effects on osteoclast differentiation and anti-osteoclast function of ECH was performed by inhibiting NFATc1 expression through the PI3K/Akt/c-Fos signaling pathway.

However, our study does have limitations. First, although the PJI rat model established in this study is not a classical osteolysis disease model, PJI often occurs in postoperative complications in TJA patients clinically and accurately reflect the pathological changes of inflammatory osteolysis caused by infection. Therefore, the PJI model we used to explore the therapeutic drugs for inflammatory osteolysis is reliable. We plan to address this limitation by subsequently additional preclinical studies in ovariectomy-induced osteoporosis, bone defect, or fracture repair. Second, although previous studies have indicated that ECH has certain anti-inflammatory effects, this study aimed to explore the inhibitory effects of ECH on osteoclast activity and infected osteolysis after debridement in PJI rats. We planned to perform subsequent studies on the combined administration of ECH and antibiotics on infection treatment, inhibition of osteoclasts activities and infected osteolysis.

## 5 CONCLUSION

Our study showed that ECH inhibited RANKL-induced osteoclast differentiation and bone resorption function. The mechanism was that ECH inhibited c-Fos expression by down-regulating PI3K expression and Akt phosphorylation. This effect subsequently down-regulated the expression of the downstream nuclear transcription factor NFATc1 and led to the

inhibition of osteoclast marker gene *Acp5*, *CtsK* expression. This data suggested that ECH was expected to be an effective therapeutic agent for inflammatory osteolysis (Figure 7).

## DATA AVAILABILITY STATEMENT

The original contributions presented in the study are included in the article/Supplementary Material, further inquiries can be directed to the corresponding author.

## ETHICS STATEMENT

The animal study was reviewed and approved by Committee on the Ethics of Animal Experiments of the School of Medicine, Wuhan University. All animal experimental procedures were performed following the Guidelines for the Care and Use of Laboratory Animals of the Chinese Animal Welfare Committee

## REFERENCES

- Aggarwal, V. K., Bakhshi, H., Ecker, N. U., Parvizi, J., Gehrke, T., and Kendoff, D. (2014). Organism Profile in Periprosthetic Joint Infection: Pathogens Differ at Two Arthroplasty Infection Referral Centers in Europe and in the United States. *J. Knee Surg.* 27 (5), 399–406. doi:10.1055/s-0033-1364102
- Ahern, E., Smyth, M. J., Dougall, W. C., and Teng, M. W. L. (2018). Roles of the RANKL-RANK axis in Antitumour Immunity - Implications for Therapy. *Nat. Rev. Clin. Oncol.* 15 (11), 676–693. doi:10.1038/s41571-018-0095-y
- Awasanya, O. D., Dalloul, C. E., Blosser, R. J., Dadwal, U. C., Carozza, M., Boschen, K., et al. (2022). Osteoclast-mediated Bone Loss Observed in a COVID-19 Mouse Model. *Bone* 154, 116227. doi:10.1016/j.bone.2021.116227
- Baek, J. M., Kim, J. Y., Yoon, K. H., Oh, J., and Lee, M. S. (2016). Ebselen Is a Potential Anti-osteoporosis Agent by Suppressing Receptor Activator of Nuclear Factor Kappa-B Ligand-Induced Osteoclast Differentiation *In Vitro* and Lipopolysaccharide-Induced Inflammatory Bone Destruction *In Vivo*. *Int. J. Biol. Sci.* 12 (5), 478–488. doi:10.7150/ijbs.13815
- Bian, P., Liu, C., Hu, W., Ding, Y., Qiu, S., and Li, L. (2021). Echinacoside Suppresses the Progression of Breast Cancer by Downregulating the Expression of miR-4306 and miR-4508. *Integr. Cancer Ther.* 20, 15347354211062639. doi:10.1177/15347354211062639
- Bouxein, M. L., Boyd, S. K., Christiansen, B. A., Goldberg, R. E., Jepsen, K. J., and Müller, R. (2010). Guidelines for Assessment of Bone Microstructure in Rodents Using Micro-computed Tomography. *J. Bone Min. Res.* 25 (7), 1468–1486. doi:10.1002/jbmr.141
- Cahill, J. L., Shadbolt, B., Scarvell, J. M., and Smith, P. N. (2008). Quality of Life after Infection in Total Joint Replacement. *J. Orthop. Surg. Hong. Kong* 16 (1), 58–65. doi:10.1177/230949900801600115
- Chuang, H. W., Wang, T. Y., Huang, C. C., and Wei, I. H. (2022). Echinacoside Exhibits Antidepressant-like Effects through AMPAR-Akt/ERK-mTOR Pathway Stimulation and BDNF Expression in Mice. *Chin. Med.* 17 (1), 9. doi:10.1186/s13020-021-00549-5
- Dapunt, U., Giese, T., Maurer, S., Stegmaier, S., Prior, B., Hänsch, G. M., et al. (2015). Neutrophil-derived MRP-14 Is Up-Regulated in Infectious Osteomyelitis and Stimulates Osteoclast Generation. *J. Leukoc. Biol.* 98 (4), 575–582. doi:10.1189/jlb.3VMA1014-482R
- Fleischmann, A., Hafezi, F., Elliott, C., Remé, C. E., Rütther, U., and Wagner, E. F. (2000). Fra-1 Replaces C-fos-dependent Functions in Mice. *Genes Dev.* 14 (21), 2695–2700. doi:10.1101/gad.187900
- Gallego-Escuredo, J. M., Lamarca, M. K., Villarroya, J., Domingo, J. C., Mateo, M. G., Gutierrez, M. D. M., et al. (2017). High FGF21 Levels Are Associated with Altered Bone Homeostasis in HIV-1-Infected Patients. *Metabolism* 71, 163–170. doi:10.1016/j.metabol.2017.03.014
- Gong, W., Zhang, N., Cheng, G., Zhang, Q., He, Y., Shen, Y., et al. (2019). Rehmannia Glutinosa Libosch Extracts Prevent Bone Loss and Architectural Deterioration and Enhance Osteoblastic Bone Formation by Regulating the IGF-1/PI3K/mTOR Pathway in Streptozotocin-Induced Diabetic Rats. *Int. J. Mol. Sci.* 20 (16). doi:10.3390/ijms20163964
- Gu, L., Lian, D., Zheng, Y., Zhou, W., Gu, J., and Liu, X. (2020). Echinacoside-induced N-itrated O-xide P-rodution in E-ndothelial cells: Roles of A-ndrogen R-eceptor and the PI3K-Akt P-athtway. *Int. J. Mol. Med.* 45 (4), 1195–1202. doi:10.3892/ijmm.2020.4476
- Han, S. Y., and Kim, Y. K. (2019). Berberine Suppresses RANKL-Induced Osteoclast Differentiation by Inhibiting C-Fos and NFATc1 Expression. *Am. J. Chin. Med.* 47 (2), 439–455. doi:10.1142/S0192415X19500228
- Hayman, A. R. (2008). Tartrate-resistant Acid Phosphatase (TRAP) and the Osteoclast/immune Cell Dichotomy. *Autoimmunity* 41 (3), 218–223. doi:10.1080/08916930701694667
- Hodges, N. A., Sussman, E. M., and Stegemann, J. P. (2021). Aseptic and Septic Prosthetic Joint Loosening: Impact of Biomaterial Wear on Immune Cell Function, Inflammation, and Infection. *Biomaterials* 278, 121127. doi:10.1016/j.biomaterials.2021.121127
- Jia, Y., Jiang, J., Lu, X., Zhang, T., Zhao, K., Han, W., et al. (2019). Garcinol Suppresses RANKL-Induced Osteoclastogenesis and its Underlying Mechanism. *J. Cell. Physiol.* 234 (5), 7498–7509. doi:10.1002/jcp.27511
- Jiang, W., Rixiati, Y., Huang, H., Shi, Y., Huang, C., and Jiao, B. (2020). Asperolide A Prevents Bone Metastatic Breast Cancer via the PI3K/AKT/mTOR/c-Fos/NFATc1 Signaling Pathway. *Cancer Med.* 9 (21), 8173–8185. doi:10.1002/cam4.3432
- Li, F., Yang, Y., Zhu, P., Chen, W., Qi, D., Shi, X., et al. (2012). Echinacoside Promotes Bone Regeneration by Increasing OPG/RANKL Ratio in MC3T3-E1 Cells. *Fitoterapia* 83 (8), 1443–1450. doi:10.1016/j.fitote.2012.08.008
- Li, K., Zhuang, P., Tao, B., Li, D., Xing, X., and Mei, X. (2020). Ultra-Small Lysozyme-Protected Gold Nanoclusters as Nanomedicines Inducing Osteogenic Differentiation. *Int. J. Nanomedicine* 15, 4705–4716. doi:10.2147/IJN.S241163
- Li, L., Wan, G., Han, B., and Zhang, Z. (2018). Echinacoside Alleviated LPS-Induced Cell Apoptosis and Inflammation in Rat Intestine Epithelial Cells by Inhibiting the mTOR/STAT3 Pathway. *Biomed. Pharmacother.* 104, 622–628. doi:10.1016/j.biopha.2018.05.072
- Liu, C., Wang, L., Zhu, R., Liu, H., Ma, R., Chen, B., et al. (2019). Rehmanniae Radix Preparata Suppresses Bone Loss and Increases Bone Strength through Interfering with Canonical Wnt/ $\beta$ -Catenin Signaling Pathway in OVX Rats. *Osteoporos. Int.* 30 (2), 491–505. doi:10.1007/s00198-018-4670-y

## AUTHOR CONTRIBUTIONS

TJ and HG designed and performed the research, analyzed the data and prepared the manuscript. JW designed and performed the research, analyzed the data and revised the paper.

## ACKNOWLEDGMENTS

The authors thank HG, Department of Orthopedic Surgery, Zhongnan Hospital of Wuhan University, for his invaluable technical assistance.

## SUPPLEMENTARY MATERIAL

The Supplementary Material for this article can be found online at: <https://www.frontiersin.org/articles/10.3389/fphar.2022.930053/full#supplementary-material>

- Liu, J., Tang, N., Liu, N., Lei, P., and Wang, F. (2022). Echinacoside Inhibits the Proliferation, Migration, Invasion and Angiogenesis of Ovarian Cancer Cells through PI3K/AKT Pathway. *J. Mol. Histol.* 53, 493–502. doi:10.1007/s10735-022-10073-x
- Liu, W., Zhou, J., Niu, F., Pu, F., Wang, Z., Huang, M., et al. (2020). *Mycobacterium tuberculosis* Infection Increases the Number of Osteoclasts and Inhibits Osteoclast Apoptosis by Regulating TNF- $\alpha$ -Mediated Osteoclast Autophagy. *Exp. Ther. Med.* 20 (3), 1889–1898. doi:10.3892/etm.2020.8903
- Lu, C. W., Lin, T. Y., Huang, S. K., and Wang, S. J. (2016). Echinacoside Inhibits Glutamate Release by Suppressing Voltage-dependent Ca(2+) Entry and Protein Kinase C in Rat Cerebrocortical Nerve Terminals. *Int. J. Mol. Sci.* 17 (7). doi:10.3390/ijms17071006
- Marchisio, P. C., Cirillo, D., Naldini, L., Primavera, M. V., Teti, A., and Zamboni-Zallone, A. (1984). Cell-substratum Interaction of Cultured Avian Osteoclasts Is Mediated by Specific Adhesion Structures. *J. Cell Biol.* 99 (5), 1696–1705. doi:10.1083/jcb.99.5.1696
- Mundy, G. R. (2007). Osteoporosis and Inflammation. *Nutr. Rev.* 65 (12 Pt 2), S147–S151. doi:10.1111/j.1753-4887.2007.tb00353.x
- Ni, Y., Deng, J., Liu, X., Li, Q., Zhang, J., Bai, H., et al. (2021). Echinacoside Reverses Myocardial Remodeling and Improves Heart Function via Regulating SIRT1/FOXO3a/MnSOD axis in HF Rats Induced by Isoproterenol. *J. Cell. Mol. Med.* 25 (1), 203–216. doi:10.1111/jcmm.15904
- Redlich, K., and Smolen, J. S. (2012). Inflammatory Bone Loss: Pathogenesis and Therapeutic Intervention. *Nat. Rev. Drug Discov.* 11 (3), 234–250. doi:10.1038/nrd3669
- Romanò, C. L., Romanò, D., Logoluso, N., and Drago, L. (2011). Bone and Joint Infections in Adults: a Comprehensive Classification Proposal. *Eur. Orthop. Traumatol.* 1 (6), 207–217. doi:10.1007/s12570-011-0056-8
- Rychter, A. M., Ratajczak, A. E., Szymczak-Tomczak, A., Michalak, M., Eder, P., Dobrowolska, A., et al. (2021). Associations of Lifestyle Factors with Osteopenia and Osteoporosis in Polish Patients with Inflammatory Bowel Disease. *Nutrients* 13 (6), 1863. doi:10.3390/nu13061863
- Sakurai, A., Okahashi, N., Nakagawa, I., Kawabata, S., Amano, A., Ooshima, T., et al. (2003). Streptococcus Pyogenes Infection Induces Septic Arthritis with Increased Production of the Receptor Activator of the NF- $\kappa$ B Ligand. *Infect. Immun.* 71 (10), 6019–6026. doi:10.1128/IAI.71.10.6019-6026.2003
- Suh, K. S., Rhee, S. Y., Kim, Y. S., Lee, Y. S., and Choi, E. M. (2013). Xanthohumol Modulates the Expression of Osteoclast-specific Genes during Osteoclastogenesis in RAW264.7 Cells. *Food Chem. Toxicol.* 62, 99–106. doi:10.1016/j.fct.2013.08.047
- Sun, X., Zhang, J., Wang, Z., Liu, B., Zhu, S., Zhu, L., et al. (2019). Licorice Isoliquiritigenin-Encapsulated Mesoporous Silica Nanoparticles for Osteoclast Inhibition and Bone Loss Prevention. *Theranostics* 9 (18), 5183–5199. doi:10.7150/thno.33376
- Tang, C., Gong, L., Lvzi Xu, X., Qiu, K., Zhang, Z., and Wan, L. (2020). Echinacoside Inhibits Breast Cancer Cells by Suppressing the Wnt/ $\beta$ -Catenin Signaling Pathway. *Biochem. Biophys. Res. Commun.* 526 (1), 170–175. doi:10.1016/j.bbrc.2020.03.050
- Wei, J., Tong, K., Zhou, S., Wang, H., Wen, Y., and Chen, L. (2021a). Intra-wound Vancomycin Powder for the Eradication of Periprosthetic Joint Infection after Debridement and Implant Exchange: Experimental Study in a Rat Model. *BMC Microbiol.* 21 (1), 333. doi:10.1186/s12866-021-02399-5
- Wei, J., Wen, Y., Tong, K., Wang, H., and Chen, L. (2021b). Local Application of Vancomycin in One-Stage Revision of Prosthetic Joint Infection Caused by Methicillin-Resistant *Staphylococcus aureus*. *Antimicrob. Agents Chemother.* 65 (9), e0030321. doi:10.1128/AAC.00303-21
- Wei, J., Tong, K., Wang, H., Wen, Y., and Chen, L. (2022). Dosage, Efficacy, and Safety of Intra-articular Vancomycin for Prophylaxis of Periprosthetic Joint Infection Caused by Methicillin-Resistant *Staphylococcus aureus* after Total Knee Arthroplasty in a Rat Model. *Antimicrob. Agents Chemother.* 66, AAC0164121. doi:10.1128/AAC.01641-21
- Wu, C. J., Chien, M. Y., Lin, N. H., Lin, Y. C., Chen, W. Y., Chen, C. H., et al. (2019). Echinacoside Isolated from *Cistanche Tubulosa* Putatively Stimulates Growth Hormone Secretion via Activation of the Ghrelin Receptor. *Molecules* 24 (4). doi:10.3390/molecules24040720
- Ye, Y., Song, Y., Zhuang, J., Wang, G., Ni, J., and Xia, W. (2019). Anticancer Effects of Echinacoside in Hepatocellular Carcinoma Mouse Model and HepG2 Cells. *J. Cell. Physiol.* 234 (2), 1880–1888. doi:10.1002/jcp.27063
- Yeon, J. T., Kim, K. J., Son, Y. J., Park, S. J., and Kim, S. H. (2019). Idelalisib Inhibits Osteoclast Differentiation and Pre-osteoclast Migration by Blocking the PI3K $\delta$ -Akt-C-Fos/NFATc1 Signaling Cascade. *Arch. Pharm. Res.* 42 (8), 712–721. doi:10.1007/s12272-019-01163-8
- Zeng, K. W., Wang, J. K., Wang, L. C., Guo, Q., Liu, T. T., Wang, F. J., et al. (2021). Small Molecule Induces Mitochondrial Fusion for Neuroprotection via Targeting CK2 without Affecting its Conventional Kinase Activity. *Signal Transduct. Target Ther.* 6 (1), 71. doi:10.1038/s41392-020-00447-6
- Zhang, D., Lu, C., Yu, Z., Wang, X., Yan, L., Zhang, J., et al. (2017). Echinacoside Alleviates UVB Irradiation-Mediated Skin Damage via Inhibition of Oxidative Stress, DNA Damage, and Apoptosis. *Oxidative Med. Cell. Longev.* 2017–15. doi:10.1155/2017/6851464
- Zheng, H., Su, Y., Sun, Y., Tang, T., Zhang, D., He, X., et al. (2019). Echinacoside Alleviates Hypobaric Hypoxia-Induced Memory Impairment in C57 Mice. *Phytother. Res.* 33 (4), 1150–1160. doi:10.1002/ptr.6310
- Zhou, L., Yao, M., Tian, Z., Song, Y., Sun, Y., Ye, J., et al. (2020). Echinacoside Attenuates Inflammatory Response in a Rat Model of Cervical Spondylotic Myelopathy via Inhibition of Excessive Mitochondrial Fission. *Free Radic. Biol. Med.* 152, 697–714. doi:10.1016/j.freeradbiomed.2020.01.014

**Conflict of Interest:** The authors declare that the research was conducted in the absence of any commercial or financial relationships that could be construed as a potential conflict of interest.

**Publisher's Note:** All claims expressed in this article are solely those of the authors and do not necessarily represent those of their affiliated organizations, or those of the publisher, the editors and the reviewers. Any product that may be evaluated in this article, or claim that may be made by its manufacturer, is not guaranteed or endorsed by the publisher.

Copyright © 2022 Jiang, Gu and Wei. This is an open-access article distributed under the terms of the Creative Commons Attribution License (CC BY). The use, distribution or reproduction in other forums is permitted, provided the original author(s) and the copyright owner(s) are credited and that the original publication in this journal is cited, in accordance with accepted academic practice. No use, distribution or reproduction is permitted which does not comply with these terms.